JOURNAL OF GEOPHYSICAL RESEARCH, VOL. 95, NO. B5, PAGES 6943–6953, MAY 10, 1990

# Shock-Induced Temperatures of $CaMgSi_2O_6$

BOB SVENDSEN AND THOMAS J. AHRENS

*Seismological Laboratory, California Institute of Technology, Pasadena, California*

**Optical radiation from $CaMgSi_2O_6$ crystal (diopside) shock-compressed to 145-170 GPa yields shock-induced temperatures of 3500-4800 K, while that from $CaMgSi_2O_6$ glass, with a density 86% that of $CaMgSi_2O_6$ crystal, shock-compressed to 96-98 GPa, yields shock-induced temperatures of 3700-3900 K. The observed radiation histories of of the targets containing $CaMgSi_2O_6$ crystal and glass imply that the shock-compressed states of both are highly absorptive, with effective absorption coefficients of $\geq$500-1000 $m^{-1}$. Calculated shock-compressed states for both $CaMgSi_2O_6$ crystal and glass, when compared to experimental results, imply the presence of a high-pressure phase (HPP) along both Hugoniots over the respective pressure ranges. The $CaMgSi_2O_6$ crystal experimental results are consistent with a standard temperature and pressure (STP) HPP mass density of 4100±100 kg/$m^3$, a STP HPP bulk modulus of 250±50 GPa, and a difference in specific internal energy (SIE) between (metastable) HPP and the $CaMgSi_2O_6$ crystal states at STP ("energy of transition") of 2.2±0.5 MJ/kg. The $CaMgSi_2O_6$ glass results are "best-fit" by the same (median) values of all three parameters; except for the STP SIE difference between the $CaMgSi_2O_6$ glass and HPP states, however, they are less sensitive to parameter variations than the crystal results because they are at lower pressure. All these model constraints are insensitive to the range of values (1-2) assumed for the STP HPP Grüneisen's parameter. The relatively high value of the STP SIE difference between HPP and $CaMgSi_2O_6$ crystal or glass most likely implies that $CaMgSi_2O_6$ glass and crystal experience both solid-solid and solid-liquid phase transformations along their respective Hugoniots below 96 and 144 GPa, respectively. The HPP $CaMgSi_2O_6$ Hugoniot constrained by the crystal experimental results lies between 2500-3000 K in the pressure range (110-135 GPa) of the lowermost mantle ($D''$); our results imply that $CaMgSi_2O_6$ is at least partly molten at these pressures and temperatures. Seismically constrained compositional models for this region of Earth's lower mantle suggest that it could contain a significant amount of Ca (25-30 wt % CaO). If so, our results imply that the temperature of the $D''$ region must be below ≈3000 K, since the finite S-wave velocity of the $D''$ region implies that it must be (at least at seismic frequencies) predominantly solid.**

## INTRODUCTION

Mg-Fe oxides and/or silicates are currently believed to compose most of Earth's mantle, but other cations, such as Ca and Al, may also be important in the upper mantle and $D''$. If so, $CaMgSi_2O_6$ (diopside) represents one of the end-member pyroxenes potentially relevant to the composition of the mantle; it is the only pyroxene that forms relatively large, transparent single crystals suitable for shock temperature investigations. The possibility that Earth accreted inhomogeneously [e.g., *Turekian and Clark*, 1969], or differentiated during core formation [e.g., *Stevenson*, 1981], implies that certain regions of the mantle, such as $D''$, may contain significant amounts of (Ca, Al)-bearing (i.e., more refractory) oxides and/or silicates. Equilibrium condensation calculations imply that $CaMgSi_2O_6$ (Di) is likely to have been one of the earliest phases to condense out of the solar nebula [*Grossman and Larimer*, 1974]. A number of previous static and dynamic experimental efforts [e.g., *Liu*, 1978, 1979*a*, 1987; *Svendsen and Ahrens*, 1983; *Boslough et al.*, 1984, 1986] and modeling efforts [e.g., *Ruff and Anderson*, 1980] have directly or indirectly addressed this issue. In this paper, we use the shock-induced radiation from Di to constrain the temperature (T) of its shock-compressed (Hugoniot) states. Combining these constraints with previous work on the pressure (P)-density ($\varrho$) Hugoniot of Di, we place constraints on the high-pressure phase relations in the $CaMgSi_2O_6$ system, and then compare these to existing mantle TP models.



Paper number 88JB03952.
0148-0227/90/88JB-03952$05.00

## EXPERIMENTAL METHODS

We performed the experiments on a two-stage, light-gas gun [e.g., *Jeanloz and Ahrens*, 1980*a*] (Figure 1). In these experiments, a lexan-encased tantalum (Ta) flyer plate, accelerated to velocities between 4.7 and 6.1 km/s (Table 4), impacted a 1.5-mm-thick Ta driver plate in contact with an ≈2-mm-thick transparent Di crystal sample or a 4-mm-thick transparent Di glass sample (Table 4). We covered the free surface of the samples with an aluminum ring to block out radiation from the target's edge and so restrict observed radiation to that coming from the center of the target. Radiation from the target reflects from a mirror, propagates through an objective lens, and is directed by (dichroic) pellicle, and and two half-silvered, beam splitters into four detectors filtered at nominal wavelengths of 450, 600, 750, and 900 nm. We recorded the signal from each detector with a Tektronix 485 single-sweep oscilloscope and a LeCroy (model 8081) 100-MHz transient recorder.

The measured densities of Di crystal samples (Table 4) agree well with the crystal value of 3277 kg/$m^3$ given by *Robie et al.* [1978]. Also, the microprobe analyses of our samples (Table 1) indicate that they each have a nearly ideal composition. The Di glass samples are 13.7% less dense than the crystal samples; this is consistent with other measured Di glass densities [*Binsted et al.*, 1985].

As in previous studies [e.g., *Lyzenga*, 1980; *Boslough et al.*, 1984], we vapor-deposited 500-1000 nm of silver (Ag) on the sample, and then placed the Ag film in mechanical contact with the Ta driver plate to minimize localized dissipation and reshocking at the driver plate-sample interface. In principle, the Ag film should absorb any radiation from the Ta-Ag interface, and heat up much less than a

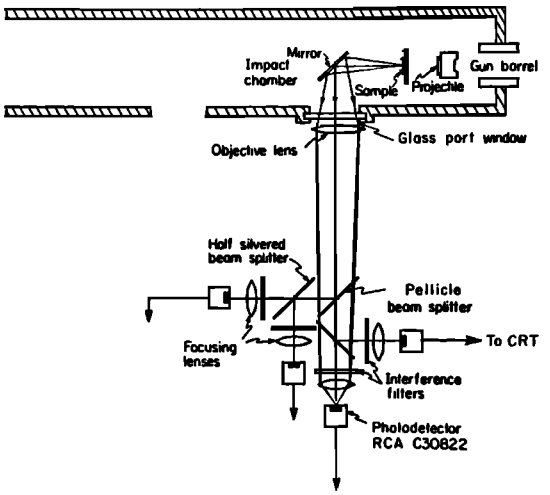


Fig. 1. Geometry of the light-gas gun radiation experiment after *Boslough* [1984]. The projectile, shot through the barrel, impacts the sample at velocities between 4.6 and 6.1 km/s. Radiation from the sample is turned 90° by the mirror, travels through the objective lens, and is split by three beam splitters amongst the four channels of the pyrometer. The resulting signals from the photodiode in each channel are monitored by oscilloscopes and LeCroy transient digital recorders.

mechanical Ta-Di interface [*Urtiew and Grover*, 1974]. Using a vacuum-formed interface is also advantageous because the mechanically formed interface could contain trapped gas that might contribute to observable radiation from the driver plate-sample interface [*Boslough*, 1984].

## DATA ANALYSIS

Our data set consists of six experiments: four on diopside single crystals (140, 141, 169, and 170, Table 4), and two on $CaMgSi_2O_6$ glass (196 and 197, Table 4). We record the radiation intensity from the target as a function of time at the wavelengths stated above. Figures 2*a* and 2*b*, displaying examples of these data at 750 nm, are representative of the radiation history observed in all Di glass and crystal experiments, respectively (Table 4), and at all other recorded wavelengths (e.g., 450, 600 and 900 nm). With the known radiation intensity of a standard lamp at the observed wavelengths [*Boslough*, 1984], we transformed the raw data displayed in Figures 2*a* and 2*b* into experimental spectral radiation intensities (i.e., spectral radiance) as a function of time. The data for all experiments, in this (reduced) spectral radiance form, are listed in Table 2.

Both the interpretation of the observed radiation histories, and the quantitative results that follow, depend upon the following model for radiative transport in the experimental targets [*Boslough*, 1985; *Svendsen et al.*, 1989]. Assuming that the target may be represented optically as a set of plane-parallel layers in contact at optically smooth interfaces, we interpret the observed spectral radiation intensity $I_{\lambda esp}(\lambda, t)$ in the context of a model intensity $I_{\lambda mod}(\lambda, t)$ as a function of radiation wavelength $\lambda$ and time after the onset of radiation from the target $t$:

$$I_{\lambda mod}(\lambda, t) = \hat{\epsilon}_{\lambda I}(t)\, I_{\lambda Pl}[\lambda, T_I(t)] + \hat{\epsilon}_{\lambda S}(t)\, I_{\lambda Pl}(\lambda, T_S) \quad (1)$$

In this last relation,

$$I_{\lambda Pl}(\lambda, t) = \frac{C_1}{\lambda^5 (e^{C_2/\lambda T} - 1)} \quad (2)$$

is the Planck function, with $C_1 = 1.19088 \times 10^{-16}$ Wm$^2$ and $C_2 = 1.4488 \times 10^{-2}$ mK, $T_S$ is the shock-compressed (Hugoniot) sample (i.e., Di crystal or glass) temperature, which is assumed homogeneous, uniform, and constant, $T_I(t)$ is the temperature of Ag at the Ag-sample interface, which may be time dependent [*Grover and Urtiew*, 1974],

$$\hat{\epsilon}_{\lambda I}(t) = \mathcal{T}_\lambda(t) r_{\lambda S}(t)[1 - r_{\lambda I}] \quad (3)$$

is the effective normal spectral emissivity of Ag at the Ag-Di interface, and

$$\hat{\epsilon}_{\lambda S}(t) = \mathcal{T}_\lambda(t)[1 + r_{\lambda I} r_{\lambda S}(t)][1 - r_{\lambda S}(t)] \quad (4)$$

is that of shocked Di, with

$$\mathcal{T}_\lambda(t) = [1 - r_{\lambda FS}] r_{\lambda US}(t)[1 - r_{SF}] \quad (5)$$

The parameters $r_{\lambda FS}$, $r_{SF}$, and $r_{\lambda I}$ in (3) and (4) are the effective normal spectral reflectivities of the unshocked sample free surface, shock front, and Ag-sample interface, respectively. Further,

$$r_{\lambda US}(t) = \exp\{-a^*_{\lambda US}\,(1 - t/t_{esp})\} \quad (6)$$

TABLE 1. Microprobe Analyses of Starting Materials

| Oxide | Shots 140, 141[a] | Shots 169, 170[b] | Shots 196, 197[c] |
|---|---|---|---|
| $Na_2O$ | 0.38[d] | 0.48 | 0.39 |
| MgO | 17.40 | 17.63 | 17.59 |
| $Al_2O_3$ | 0.36 | 0.22 | 0.36 |
| $SiO_2$ | 55.74 | 55.32 | 56.08 |
| CaO | 25.15 | 24.78 | 25.30 |
| $TiO_2$ | 0.02 | 0.11 | 0.02 |
| $Cr_2O_3$ | 0.07 | 0.48 | 0.02 |
| MnO | 0.08 | 0.04 | 0.06 |
| FeO | 0.82 | 0.96 | 0.81 |
| Total | 99.97 | 99.68 | 100.63 |
| En | 48.4 | 49.0 | 48.4 |
| Wo | 50.3 | 49.5 | 50.3 |
| Fs | 1.4 | 1.5 | 1.4 |

[a] Diopside from DeKalb, NY, supplied by S. Huebner, U. S. Geological Survey, Reston, Virginia.
[b] Russian diopside, supplied by Gem Obsessions, San Diego, California.
[c] Diopside glass, supplied by G. Miller, Caltech, and G. Fine, Corning Glass Co.
[d] Weight %.

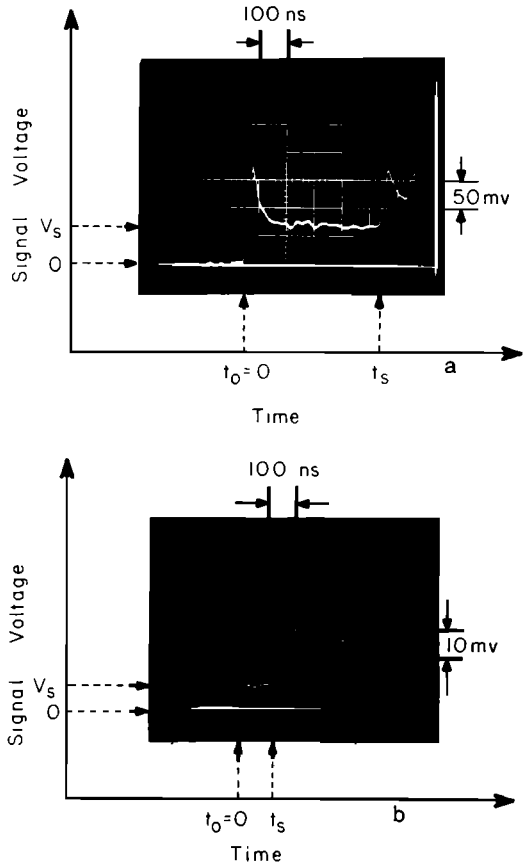


Fig. 2. Radiation intensity versus time record (a) for shot 197 on Di glass, and (b) for shot 141 on Di single crystal, both at 750 nm. The duration of the radiation intensity from the shocked crystal is much shorter than that from the glass because the crystal sample is much thinner (Table 4).

is the effective normal spectral transmissivity of the unshocked sample layer, and

$$\tau_{\lambda S}(t) = \exp\{-a^*_{\lambda S}\, t/t_{exp}\} \tag{7}$$

is that of the shocked sample layer. The quantities $a^*_{\lambda US}$ and $a^*_{\lambda S}$ are nondimensional forms of the effective normal spectral absorption coefficients $a_{\lambda US}$ and $a_{\lambda S}$, respectively, of the unshocked and shocked sample layers, respectively, defined by

$$a^*_{\lambda US} = a_{\lambda US}(u_S - v_{HS})t_{exp} \tag{8}$$

and

$$a^*_{\lambda S} = a_{\lambda S}\, u_S\, t_{exp} \tag{9}$$

The parameter $t_{exp} = d/u_S$ is the experimental time scale (i.e., $t_S - t_O$, Figure 2*a* or 2*b*), $u_S$ is the velocity of the shock front through the sample, $v_{HS}$ is the material velocity of the shocked sample material (i.e., Di crystal or glass), and $d$ is the initial thickness of the sample layer in the target. Note that we have set the material velocity of the unshocked sample material equal to zero in writing (8) and (9) to be consistent with our experiments. Bearing in mind that all optical properties in the expressions above are spectral quantities, as designated by the subscript $\lambda$, we drop this subscript in the following development to simplify notation. So, unless otherwise noted, all model optical properties are spectral.

As stated above, the target consists of a Ta driver plate, Ag film layer, and sample layer. In principle, radiation from the target is first observed when the shock wave compresses the Ag film at the Ag-sample interface ($t_o$, Figure 2*a* or 2*b*). As shown most clearly in Figure 2*a*, the radiation intensity in all Di experiments rises sharply to a peak value, and then, as the shock wave propagates into the sample, the intensity decays almost as quickly to an approximately time independent value. This occurs over 100-110 ns (Figure 2*a*) to the radiation intensity from Di glass targets, and over 20-30 ns (Figure 2*b*) to the radiation intensity from Di crystal targets. From the model relations (1)-(4), we see that $T_I(t)$, $\tau_S(t)$, and $\tau_{US}(t)$ are, in general, time dependent. Of these, only $T_I(t)$ and $\tau_S(t)$ may decrease with time; $\tau_{US}(t)$ increases with time (for $a^*_{US} \geq 0$), as can be seen from (6). Although the time dependence of $I_{exp}(\lambda, t)$ can be explained by $T_I(t)$, as shown by thermal conduction models [*Grover and Urtiew*, 1974; *Svendsen et al.*, 1989] for the experimental targets, conduction model calculations imply that the temperatures we infer from $I_{exp}(\lambda, t)$ via the model below (relation (14)) are implausibly low to represent $T_I(t)$. These models imply that the Ag-Di interface temperature, $T_I(t)$, is bounded below by its value for $t \to \infty$, given by

$$T_I(t) > T_I(\infty) = \frac{1}{(1+\sigma)}(T_F + \sigma T_S) \tag{10}$$

In this relation, $T_F$ is the temperature of the release state of the Ag film, at the same pressure as the shock-compressed Di crystal or glass,

$$\sigma = \left\{\frac{k_S \varrho_S c_{PS}}{k_F \varrho_F c_{PF}}\right\}^{1/2} \tag{11}$$

is the "thermal inertial" mismatch between the released Ag film and shock-compressed Di crystal or glass; $k_F$, $\varrho_F$, and $c_{PF}$ are the thermal conductivity, density and specific heat at constant pressure, respectively, of the released Ag film, and $k_S$, $\varrho_S$, and $c_{PS}$ are the analogous properties of the shock-compressed Di crystal or glass. In the relevant pressure range (150-170 GPa), calculations for this kind of target suggest that $T_F \gtrsim 10^4$ K [*Svendsen and Ahrens*, 1987], and Hugoniot calculations presented below for Di suggest $T_S \sim 4000$ K; in this case, we need $\sigma \gtrsim 10$ to have $T_I(\infty) \lesssim T_S$. However, estimates of the parameters composing $\sigma$ [*Svendsen and Ahrens*, 1987] for Ag and Di suggest that $\varrho_F c_{PF} \approx \varrho_S c_{PS}$ and $k_F \gtrsim 10^3 k_S$, such that $\sigma \lesssim 0.03$. On this basis, it is highly unlikely that $T_I(t)$ will decrease much below $T_F$ on the time scale of the experiments. Therefore, we conclude that the strong decay of the initial radiation intensity is controlled by $a_S \to \tau_S(t)$ and its effect on $\hat{\epsilon}_S(t)$ via (4), and reflects an increase in the optical absorption of Di upon shock compression ($a_S >> a_{US}$: [*Boslough*, 1985]). With the likely exception of $Al_2O_3$ [*Bass et al.*, 1987], all initially transparent materials studied so far (for example, LiF [*Kormer*, 1968] and $CaAl_2Si_2O_8$ [*Boslough et al.*, 1986]) lose some transparency during shock compression. In the present case, we conclude that the radiation from Ag at the Ag-Di interface is strongly absorbed by the shocked Di such that, as the shocked Di sample layer grows, the interface contribution to the observed radiation intensity is quickly reduced below that of the shocked sample, which, being constant in time, results in a time independent observed radiation history. Hence we observe the fast decay of the initial high intensity and subsequent, nearly

TABLE 2. Radiation Data and Fits.

| | Spectral Radiance ($kW/m^2$ sr nm) | | | | Fits | | | | |
|---|---|---|---|---|---|---|---|---|---|
| Shot | 450 nm | 600 nm | 750 nm | 900 nm | Parameter($t_r$, ns) | Wien | GS[a] | LM[b] | GS($\hat{\epsilon}_S = 1$) |
| 140 | | 3.15 | 3.09 | 2.87 | $\hat{\epsilon}_S(140)$ | 0.65 | 0.59 | 0.56 | |
| | | (0.59) | (0.45) | (0.81) | | (0.37) | (0.37) | (0.23) | |
| | | | | | $T_S(140)$ | 4152 | 4215 | 4270 | 3803 |
| | | | | | | (351) | (364) | (356) | (293) |
| | | | | | $\chi^2$ | 0.14 | 0.06 | 0.06 | 0.05 |
| 141 | 6.14 | 5.38 | 6.06 | 5.71 | $\hat{\epsilon}_S(145)$ | 0.71 | 0.65 | 0.75 | |
| | (1.21) | (1.00) | (0.77) | (0.93) | | (0.34) | (0.34) | (0.11) | |
| | | | | | $T_S(145)$ | 4737 | 4782 | 4643 | 4372 |
| | | | | | | (346) | (356) | (153) | (297) |
| | | | | | $\chi^2$ | 3.44 | 3.13 | 3.05 | 3.55 |
| 169 | 5.11 | 6.58 | 6.53 | 5.49 | $\hat{\epsilon}_S(198)$ | 0.91 | 0.86 | 0.86 | |
| | (0.18) | (0.31) | (0.33) | (0.31) | | (0.27) | (0.27) | (0.18) | |
| | | | | | $T_S(198)$ | 4522 | 4552 | 4555 | 4428 |
| | | | | | | (263) | (268) | (178) | (251) |
| | | | | | $\chi^2$ | 0.30 | 0.21 | 0.21 | 0.48 |
| 170 | 0.82 | 1.56 | 2.34 | 2.29 | $\hat{\epsilon}_S(170)$ | 1.01 | 1.04 | 1.06 | |
| | (0.13) | (0.17) | (0.26) | (0.26) | | (0.25) | (0.25) | (0.17) | |
| | | | | | $T_S(170)$ | 3539 | 3508 | 3498 | 3539 |
| | | | | | | (143) | (141) | (90) | (143) |
| | | | | | $\chi^2$ | 1.61 | 1.43 | 1.42 | 1.52 |
| 196 | 1.35 | 2.14 | 2.96 | 3.24 | $\hat{\epsilon}_S(485)$ | 1.09 | 1.23 | 1.63 | |
| | (0.48) | (0.33) | (0.42) | (0.51) | | (0.44) | (0.44) | (0.26) | |
| | | | | | $T_S(485)$ | 3695 | 3585 | 3422 | 3711 |
| | | | | | | (243) | (231) | (100) | (247) |
| | | | | | $\chi^2$ | 1.99 | 1.20 | 1.03 | 1.72 |
| 197 | 1.37 | 3.18 | 3.46 | 3.74 | $\hat{\epsilon}_S(475)$ | 1.51 | 1.51 | 1.38 | |
| | (0.41) | (0.39) | (0.50) | (0.56) | | (0.39) | (0.39) | (0.22) | |
| | | | | | $T_S(475)$ | 3610 | 3610 | 3663 | 3866 |
| | | | | | | (208) | (208) | (98) | (239) |
| | | | | | $\chi^2$ | 0.50 | 0.50 | 0.46 | 1.23 |

Numbers in parentheses under measured or calculated values represent uncertainties.
[a]Golden Section Search Fit: quoted uncertainties represent propagated measurement uncertainties, and this fit is unweighted.
[b]Levenberg-Marquardt Fit: quoted uncertainties represent standard deviations of fits, and this fit is weighted.

time independent, radiation intensity displayed in Figures 2*a* and 2*b*.

For the shocked sample to be strongly absorptive, we must have $a_S^* > 1$, or $a_S > 1/(d - v_{HS}t_{exp})$ from (8). Under this condition, (7) implies that $\tau_S(t) \sim 0$, and with this, $\hat{\epsilon}_I(t) \sim 0$ from (3), and

$$\hat{\epsilon}_S(t) \sim \mathcal{T}(t) = [1 - \tau_{FS}]\tau_{US}(t)[1 - \tau_{SF}] \quad (12)$$

from (4) and (5). From absorbance analyses of the Di glass and crystal samples, we also note that $a_{US} \sim 0$, and so $\tau_{US}(t) \sim 1$ via (6). Placing this into (12), we have

$$\hat{\epsilon}_S(t) \longrightarrow \hat{\epsilon}_S = [1 - \tau_{FS}][1 - \tau_{SF}] \quad (13)$$

which is also the upper bound to $\hat{\epsilon}_S(t)$, as given by (4) with $\tau_S(t) \sim 0$. Under these circumstances, we conclude that $\hat{\epsilon}_S$ for Di crystal and glass is approximately independent of time. The minimum values of $a_S$ required by the condition $a_S > 1/(d - v_{HS}t_{exp})$ may be calculated from the experimental parameters listed in Table 4. The results of this calculation, also listed in Table 4, imply that $a_S > 650$-$1100$ $m^{-1}$ and 420 $m^{-1}$ for Di crystal and glass, respectively.

Substituting the conditions $\hat{\epsilon}_I(t) = 0$ and (13) into (1), we obtain

$$I_{mod}(\lambda, t) \rightarrow I_{mod}(\lambda, T_S) = \hat{\epsilon}_S I_{Pl}(\lambda, T_S) \quad (14)$$

which represents a constant radiation intensity at a given wavelength, just as we observe in the latter part of the radiation histories (Figures 2*a* and 2*b*). Within the context of our interpretation of the observed radiation histories, (14) represents a model for the radiation from the shocked Di sample layer. Further, in view of (1), equation (14) as such a model is most likely valid at $t \approx t_{exp}$. Consequently, we use $I_{exp}(\lambda, t_{exp})$ to constrain $T_S$ via a model based on (14). In doing this, we also eliminate any influence of $a_{US}$, and so of $\tau_{\lambda US}(t)$, on the value of $T_S$ so constrained, since from (6) we see that $\tau_{US}(t) \rightarrow 1$ as $t \rightarrow t_{exp}$ for any finite value of $a_{US}$.

Since we have no model for the wavelength, pressure or temperature dependence of $\tau_{FS}$ and $\tau_{SF}$ (and so $\hat{\epsilon}_S$), we assume they are independent of these variables. In this case, (14) represents a "greybody" radiator, such that $\hat{\epsilon}_S$ becomes an independent parameter (to be constrained by the fit). Under this assumption, we fit (14) to $I_{exp}(\lambda, t_{exp})$ over $\lambda$ via a $\chi^2$ statistic [e.g., *Press et al.*, 1986, chapter 14]:

$$\chi^2(\hat{\epsilon}_S, T_S) = \sum_{n=1}^{4} [i_{exp}(\lambda_n, t_{exp}) - \hat{\epsilon}_S i_{Pl}(\lambda_n, T_S)]^2 \quad (15)$$

where $i = I/\sigma_n$ and $\sigma_n$ are the experimental uncertainties

in the radiation intensity at each wavelength. As written, the values of $\hat{\epsilon}_S$ and $T_S$ constrained by the minimization of (15) are, in general, dependent on $t_{exp}$, and so on its uncertainty. However, in our particular case, the radiation histories around $t_{exp}$ (Figures 2*a* and 2*b*) are sufficiently time independent to make this $t_{exp}$ plus uncertainty dependence negligible.

Since $I_{mod}$ is a nonlinear function of $T_S$, we find its minimum numerically using (1) Golden Section (GS) Search and (2) the method of Levenberg as formulated by Marquardt (LM: see [*Press et al.*, 1986] for details on each of these methods). We use two completely different numerical methods because we are working with a nonlinear fit. In addition, the use of two independent methods provides some assurance that our results are not dependent on the numerical technique used to obtain them. Anticipating the fit results, we note that they each give, to within experimental and/or fit uncertainty, the same values of $T_S$ and $\hat{\epsilon}_S$ (Table 2). To obtain starting values of $\hat{\epsilon}_S$ and $T_S$ for the nonlinear fit, we use Wien's approximation to $I_{Pl}(\lambda, T)$:

$$I_{W_l}(\lambda, T) = \frac{C_1}{\lambda^5} \exp\{-C_2/\lambda T\} \tag{16}$$

in $\chi^2$ as follows. Replacing $I_{Pl}(\lambda, T_S)$ with $I_{W_l}(\lambda, T_S)$ in $i_{mod}$ and taking the natural logarithm of the result, we obtain

$$\ln\{i_{mod}\} = \ln\{\sigma_n^{-1}\lambda_n^{-5}C_1\} + \ln\{\hat{\epsilon}_S\} - \frac{C_2}{T_S}\frac{1}{\lambda_n} \tag{17}$$

The data for this model is $\ln\{i_{exp}(\lambda_n, t_{exp})\}$. Replacing $i_{exp}$ and $i_{mod}$ by their natural logarithms in (15), we obtain

$$\chi^2(a,b) = \sum_{n=1}^{4}\left[\mathcal{Y}(\lambda_n, t_{exp}) - a - b\frac{1}{\lambda_n}\right]^2 \tag{18}$$

where

$$\mathcal{Y}(\lambda_n, t_{exp}) = \ln\{{C_1}^{-1}\lambda_n^5 I_{exp}(\lambda_n, t_{exp})\}$$

$a = \ln\{\hat{\epsilon}_S\}$, and $b = -C_2/T_S$. Since $\chi^2(a,b)$ is linear in $a$ and $b$ the values of these parameters (and so of $\hat{\epsilon}_S$ and $T_S$) that minimize $\chi^2$ may be found explicitly via linear least squares.

We present the results of these fits for the six experiments in Table 2, and we plot the radiation data and fits for shots 140, 169, and 197 in Figures 3*a*, 3*b*, and 3*c*, respectively. The fits labeled "Wien" in Table 2 come from (18), while the remainder come from the different numerical solutions of (15). Note that, with three or four data points and two parameters in each of these fits, a $\chi^2$ value of roughly 2 is representative of a "good" fit. This value is quite sensitive to measurement uncertainties, as can be seen from (15). In this case, the values of $\chi^2$ in Table 2 imply that we may have overestimated measurement uncertainties. In Table 2, the uncertainties quoted with the GS fits represent measurement uncertainties mapped into uncertainties for $\hat{\epsilon}_S$ and $T_S$. In contrast, the uncertainty quoted with each LM fit is the standard deviation of that fit. Note that the GS and LM fits for shot 196, and the Wien, GS, and LM fits for shots 197, give $\hat{\epsilon}_S$ values well above 1, an unphysical result. As noted by *Boslough et al.* [1986], this is not unexpected; in general, $\hat{\epsilon}_S$ is much more sensitive to data scatter than $T_S$ in the fit, given the functional form of $I_{mod}$, especially when this scatter is away from the Planck wavelength dependence [*Svendsen and Ahrens*, 1987]. All other fit and model parameters are much less sensitive to this scatter; for example, note that $T_S$ (via (2) and (15)) and $a_S^*$ (via (4) and (7) in (15), if we were fitting for it) are only logarithmically sensitive to variations in $1/I_{exp}$ and $\hat{\epsilon}_S$, respectively. Data scatter may be due to uncorrected $\lambda$ dependences in the data or experimental measurement errors. As can be seen from the corresponding GS fits in which $\hat{\epsilon}_S$ is set equal to 1, the variable $\hat{\epsilon}_S$ fits for shots 196 and 197 may underestimate the value of $T_S$ by ~200 K. Also note that the value of $\hat{\epsilon}_S$ for all experiments and all fits is >0.1, which implies that we observe relatively homogeneous radiation from both Di glass and Di crystal, as opposed to the localized, "shear band" radiation seen from many shock-compressed oxides and silicates at lower (<70 GPa) pressures [e.g., *Kondo and Ahrens*, 1983; *Schmitt et*

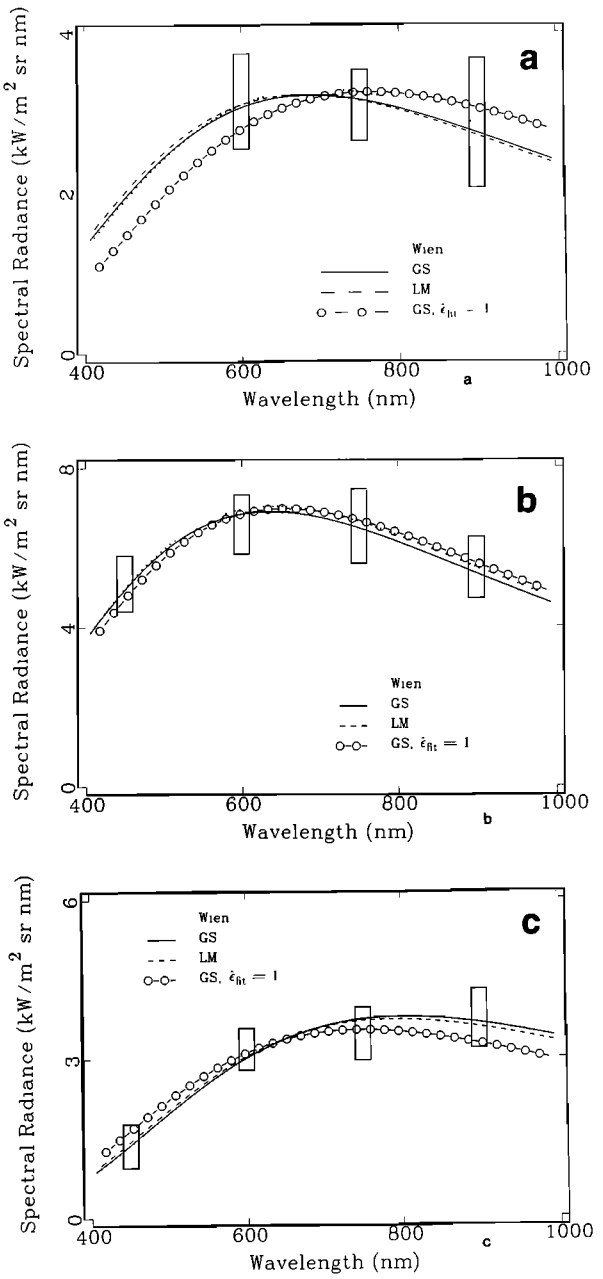


Fig. 3. Spectral radiance data versus wavelength and greybody fits for $\hat{\epsilon}_S$ and $T_S$. The size of the rectangles representing the data represents experimental uncertainty. The data for (a) shot 140, (b) shot 169, and (c) shot 197 data, are shown.

TABLE 3. $CaMgSi_2O_6$ STP Equation of State Parameters.

| Property | Symbol | Crystal | Glass | Units |
|---|---|---|---|---|
| | | *$u - v_H$ Relation* | | |
| Density | $\varrho_{i\alpha}$ | 3277[a] | 2828[b] | kg/m$^3$ |
| Intercept | $a_{i\alpha}$ | 5260[c] | 4150[d] | m/s |
| Slope | $b_{i\alpha}$ | 1.27[c] | 1.37[d] | |
| | | *High-Pressure Phase* | | |
| Density | $\varrho_i$ | 4100[c] | 4100[c] | kg/m$^3$ |
| Intercept | $a_i$ | 7826[e] | 7826[e] | m/s |
| Slope | $b_i$ | 1.22[f] | 1.22[f] | |
| Bulk Modulus | $K_{s_i}$ | 250[c] | 250[c] | GPa |
| $(\partial K/\partial P)_{s_i}$ | $K'_{s_i}$ | 3.9[c] | 3.9[c] | |
| Grüneisen's Parameter[g] | $\gamma_i$ | 1.5[c] | 1.5[c] | |
| Specific Heat[h] | $c_v$ | 1152 | 1152 | J/kg |
| HPP-LPP SIE difference | $\Delta e_i^{\beta-\alpha}$ | 2.2[i] | 2.2[i] | MJ/kg |

[a] *Robie et al.* [1978].
[b] Table 4.
[c] *Svendsen and Ahrens* [1983].
[d] See text and appendix.
[e] Assuming $a_i = \{K_{s_i}/\varrho_i\}^{1/2}$.
[f] Assuming $b_i = (1 + K'_{s_i})/4$.
[g] $\gamma\varrho$=constant used in all calculations.
[h] Dulong-Petit value, used in all calculations.
[i] From model estimates in text.

*al.*, 1986]. Although the constraint is very poor, we note that, from the association $(1 - r_{FS})(1 - r_{SF}) \approx \hat{\epsilon}_S$, as discussed above, $r_{SF} \sim 0.2$-$0.3$, with $r_{FS} \sim 0.1$, for shots 140 and 141, at least. A value of $r_{SF}$ different than zero implies a change in the index of refraction of Di across the shock front, and we tentatively conclude that this represents an increase in the index of refraction in Di upon shock compression.

## Hugoniot Calculations and Comparison with Experimental Results

Via the balance of mass and momentum between target components and and across the shock front, we calculate the material velocity $v_{H\alpha}$ of shocked target component $\alpha$ (i.e., Ta driver, Ag film, Di crystal or glass sample) using the standard impedance match assumption [*Rice et al.*, 1958] that the velocity $u_\alpha$ of the shock front through $\alpha$ is a linear function of $v_{H\alpha}$:

$$u_\alpha = a_{i\alpha} + b_{i\alpha} v_{H\alpha} \tag{19}$$

Note that $v_{i\alpha}$, the material velocity of uncompressed $\alpha$, is set to zero in writing (19), consistent with experimental conditions. Obtaining $v_{H\alpha}$ and $u_\alpha$ in this manner, the mass and momentum balances across the shock front give us the Hugoniot density $\varrho_{H\alpha}$, and pressure $P_{H\alpha}$, respectively; via the linear $u_\alpha$-$v_{H\alpha}$ assumption, these are related by

$$P_{H\alpha} = P_i + \frac{\varrho_{i\alpha} a_{i\alpha}^2 \eta_\alpha}{(1 - b_{i\alpha}\eta_\alpha)^2} \tag{20}$$

[*McQueen et al.*, 1967], i.e., the so-called shock wave equation of state.

The subscript $i$ in (19) and (20) designates a property of the initial, or uncompressed, state of each target material; with this notation, $T_i$, $P_i$, $s_{i\alpha}$, $\varrho_{i\alpha}$ and $v_{i\alpha} = 0$ are the initial temperature, pressure, specific entropy, mass density, and material velocity, respectively, of material $\alpha$. For the experiments, $T_i$ and $P_i$ are standard temperature (273 K) and pressure (0.1 MPa). We use $\varrho_{i\alpha} = 16{,}675$ kg/m$^3$, $a_{i\alpha} = 3290$ m/s and $b_{i\alpha} = 1.31$ for the Ta driver plate [*Mitchell and Nellis*, 1984], and $\varrho_{i\alpha} = 10{,}501$ kg/m$^3$, $a_{i\alpha} = 3270$ m/s and $b_{i\alpha} = 1.55$ for the Ag film [*Marsh*, 1980]. We assume that the $u_c$-$v_{Hc}$ relation for Di crystal, which is experimentally constrained to 100 GPa [*Svendsen and Ahrens*, 1983], is valid to 170 GPa (Table 3). Since, to our knowledge, there are no available Di glass $u_g$-$v_{Hg}$ data, we need to estimate the coefficients $a_{ig}$ and $b_{ig}$ of the Di glass $u_g$-$v_{Hg}$ relation, which is required, as discussed above, for calculation of the Di glass Hugoniot states achieved in the experiments. We propose to do this via a relation connecting the Di glass and crystal Hugoniots that is based on a combination of (1) an energy balance across an adiabatic shock front separating two ideal fluids (i.e., the Rankine-Hugoniot relation) and (2) equilibrium thermodynamic paths equivalent to this energy balance. Leaving the details to the appendix, we obtain ((A7) in the appendix) the following relation between crystal and glass Hugoniot states at the same Hugoniot density $\varrho_H$, occupying the same high-pressure phase (HPP):

$$P_{Hg} = \frac{(1-\phi)}{\mathcal{D}_g}\left[\mathcal{D}_c P_{Hc} + \gamma_H\left(\varrho_{ig}\Delta e_i^{g-c} + \frac{1}{2}\phi P_i\right)\right] \tag{21}$$

In this relation, $P_{Hg}$ and $P_{Hc}$ are the pressures of the glass and crystal Hugoniot states at $\varrho_H$, $\mathcal{D}_\alpha = [1 - (1 + \frac{1}{2}\gamma_H)\eta_\alpha]$, $\eta_g = 1 - \varrho_{ig}/\varrho_H$ is the relative compression of the glass, $\eta_c = 1 - \varrho_{ic}/\varrho_H$ is that of the crystal, and $\phi = 1 - \varrho_{ig}/\varrho_{ic}$. Also, $\Delta e_i^{g-c} = e(\varrho_{ig}, s_{ig}) - e(\varrho_{ic}, s_{ic})$ is the difference in specific internal energy between the glass and crystal states at $T_i$ and $P_i$, having densities $\varrho_{ig}$ and $\varrho_{ic}$, respectively, and specific entropies $s_{ig}$ and $s_{ic}$, respectively, and $\gamma_H = \gamma(\varrho_H)$, where $\gamma$ is the equilibrium thermodynamic Grüneisen's parameter of the HPP, assumed to be a function of density alone.

Equation (21) relates the pressures $P_{Hg}$ and $P_{Hc}$ along the Di glass and crystal Hugoniots, respectively, at a given

density $\varrho_H$. Via (20), we also have $P_{Hg}$ (or $P_{Hc}$) as a function of $\varrho_{Hg}$ (or $\varrho_{Hc}$) for given values of $P_i$, $\varrho_{ig}$, $a_{ig}$, and $b_{ig}$ (or $P_i$, $\varrho_{ic}$, $a_{ic}$, and $b_{ic}$). If we did have independent experimental constraints on $a_{ig}$ and $b_{ig}$, we could then use the forms given for $P_{Hg}$ and $P_{Hc}$ by (20) in (21) to constrain, for example, $\gamma_H$ (see appendix). This is, of course, not the case. Instead, we constrain values of $a_{ig}$ and $b_{ig}$ by using (21) to generate a Hugoniot for Di glass and then fitting (20) to this calculated Hugoniot between 45 and 200 GPa via the LM method used above for the experimental fits. This Hugoniot, the fit to it and consequently the values of $a_{ig}$ and $b_{ig}$ so obtained, will then in turn depend on the values of the parameters appearing in (21), i.e., $P_i$, $\Delta e_i^{g-c}$, $\varrho_{ig}$, $\varrho_{ic}$, $a_{ic}$, $b_{ic}$, $\varrho_i$ and $\gamma_i$. Leaving the details to the appendix, we use the estimates of $a_{ig}$ and $b_{ig}$ so obtained (Table 3) to calculate the impedance match for the experimental targets containing Di glass as the sample material, thereby obtaining an estimate of the Di glass $P_{Hg}$-$\varrho_{Hg}$ Hugoniot state.

Via the same kind of energy balance-equilibrium thermodynamic path relation used to obtain (21), we may estimate the temperature $T_{H\alpha}$ of a material shocked from some initial state $\{T_i, P_i, s_{i\alpha}, \varrho_{i\alpha}, v_{i\alpha} = 0\}$ to a HP state $\{T_{H\alpha}, P_{H\alpha}, s_{H\alpha}, \varrho_{H\alpha}, v_{H\alpha}\}$ and phase $\beta$ [e.g., *McQueen et al.*, 1967; *Ahrens et al.*, 1969; *Jeanloz and Ahrens*, 1980*b*; *Svendsen et al.*, 1989]:

$$T_{H\alpha} = T_{s_i} + \frac{1}{c_v(\varrho_{H\alpha})}\left[\frac{1}{2\varrho_{i\alpha}}\eta_\alpha(P_{H\alpha} + P_i) - \Delta e_{i\alpha}\right] \quad (22)$$

with $\Delta e_{i\alpha} = \Delta e_{s_i} + \Delta e_i^{\beta-\alpha}$. In this relation, $c_v(\varrho_{H\alpha})$ is the specific heat of the HPP $\beta$ at constant volume, assumed independent of temperature, $\Delta e_i^{\beta-\alpha}$ is the difference in specific internal energy between $\beta$ and $\alpha$ at $T_i$ and $P_i$, $\Delta e_{s_i}$ is the change in specific internal energy (SIE) of $\beta$ when compressed from its density at $T_i$ and $P_i$, $\varrho_i$, to $\varrho_{H\alpha}$, and $T_{s_i}$ is the temperature achieved by $\beta$ when compressed from $\varrho_i$ to $\varrho_{H\alpha}$ along its isentrope centered at $s_i = s^\beta(T_i, P_i)$. We calculate $\Delta e_{s_i} = \Delta e^\beta(\varrho_{H\alpha}; \varrho_i, K_{s_i}, K'_{s_i})$ as a function of $\varrho_i$, the HPP STP isentropic bulk modulus $K_{s_i}$, and its pressure derivative $K'_{s_i}$ via third-order Eulerian finite strain, and $T_{s_i} = T^\beta(\varrho_{H\alpha}; \varrho_i, \gamma_i)$ via $\gamma$ and the relation

$$T_{s_i} = T_i \exp\left\{\gamma_i\left[1 - \frac{\varrho_i}{\varrho_{H\alpha}}\right]\right\} \quad (23)$$

with $\gamma_i = \gamma(\varrho_i)$, under the assumption that $\gamma$ is constant, which we assume in all model calculations. With values for $\varrho_{ig}$, $\varrho_{ic}$, $a_{ic}$ and $b_{ic}$ experimentally-constrained, and $a_{ig}$ and $b_{ig}$ estimated via the procedure discussed above and in the appendix, we calculate the pressure and density of the Di crystal and glass Hugoniot states via the impedance match between target components. With these, we then calculate the temperatures of the Di crystal and glass Hugoniot states via (22) written for each, given estimates of $\varrho_i$, $\gamma_i$, and $c_v(\varrho_{H\alpha})$ for $\beta$, as well as estimates of $\Delta e_i^{\beta-c}$ for Di crystal and $\Delta e_i^{\beta-g}$ for Di glass.

The relation (22) implies that the slope of $T_{H\alpha}$ as a function of pressure or density is predominantly controlled by the dependence of $T_{H\alpha}$ on $c_v(\varrho_{H\alpha})$, while the $P_i$ "intercept" of $T_{H\alpha}$ is determined mainly by $\varrho_{i\alpha}$ and $\Delta e_i^{\beta-\alpha}$. Note that $T_{H\alpha}$ as given by (22) depends linearly on $c_v(\varrho_{H\alpha})$ and $\Delta e_i^{\beta-\alpha}$. Relations (21), (22) and (23) imply that $\gamma$ influences $T_{H\alpha}$ only indirectly. The HPP parameters $K_{s_i}$ and $K'_{s_i}$ influence $T_{H\alpha}$ through $\Delta e_{s_i}$; in particular, note that the third-order Eulerian finite strain expression for $\Delta e_{s_i}$ depends linearly on both $K_{s_i}$ and $K'_{s_i}$. The STP HPP mass density $\varrho_i$ affects $T_{H\alpha}$ (nonlinearly) through $T_{s_i}$ and $\Delta e_{s_i}$.

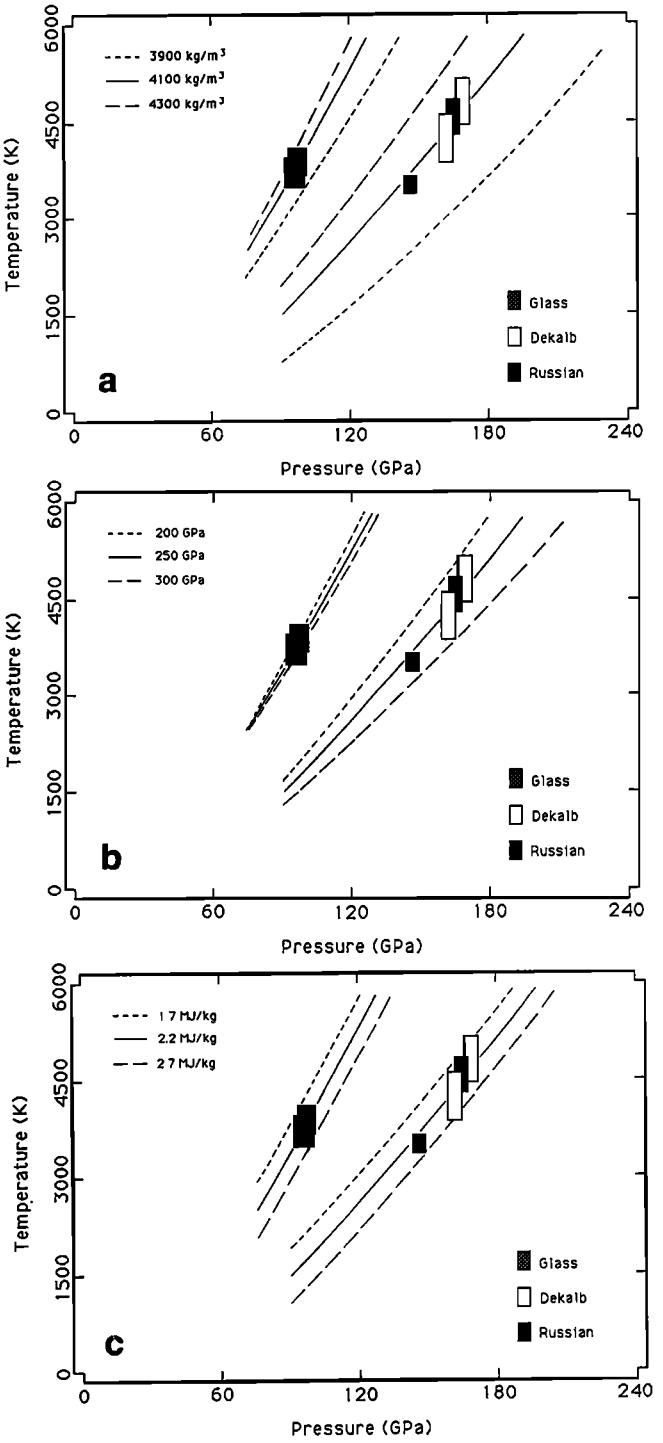


Fig. 4. Experimental results for Di crystal and glass, and model Hugoniots calculated for a range of values for the STP HPP density $\varrho_i$ (a), the STP HPP bulk modulus $K_{s_i}$ (b), and the difference in specific internal energy between the HPP and initial states at STP $\Delta e_i^{\beta-\alpha}$ (c).

In Figures 4*a*, 4*b*, and 4*c*, we display calculated Hugoniots for Di glass and crystal that are consistent with the shock temperatures constrained by the experimental results discussed in the last section. We present a range of these Hugoniots generated from a corresponding range of values for $\varrho_i$ (3900-4300 kg/m$^3$, Figure 4*a*), $K_{s_i}$ (200-300 GPa,

Figure 4*b*), and $\Delta e_i^{\beta-\alpha}$ (1.7-2.7 MJ/kg for both Di crystal and glass, Figure 4*c*), for fixed values of all parameters but the one varied, to demonstrate the relative sensitivity of $T_{H\alpha}$ to these unknowns. In all these calculations, we assume for simplicity that $c_v(\varrho_{H\alpha})$ is given by its classical lattice value, $3\nu R/M$ (Table 3), where $R$ is Ryberg's constant, and $M$ is the molecular weight (0.216553 kg/mol for Di). Values of all fixed parameters used in these calculations are given in Table 3. Note that $T_{H\alpha}(P_{H\alpha})$ varies linearly with $\Delta e_i^{\beta-\alpha}$ and $K_{s_i}$, and nonlinearly with $\varrho_i$, as discussed above. The variation of $T_{H\alpha}(P_{H\alpha})$ with $K'_{s_i}$ (not plotted) is similar to that with $K_{s_i}$. A comparison of the trend in the Di crystal experimental results with the slope of the Di crystal Hugoniots calculated in this fashion (Figures 4*a*-4*c*) suggests that the experimental trend may be slightly steeper than a $3\nu$R/M trend (i.e., $c_v(\varrho_{H\alpha}) < 3\nu$R/M for Di crystal), and so perhaps slightly pressure or temperature dependent [e.g., *Lyzenga et al.*, 1983; *Boslough et al.*, 1986]. However, there are insufficient experimental TP Hugoniot points to further constrain this possibility. The range of values used for $\varrho_i$ in Figure 4*a* $K_{s_i}$ in Figure 4*b* are based on (ideal-mixing) model oxide ($CaO+MgO+SiO_2$) and perovskite ($CaSiO_3+MgSiO_3$) solid HP assemblages for Di constrained previously from work on the $P$-$\varrho$ Hugoniot of Di [*Ahrens et al.*, 1966; *Svendsen and Ahrens*, 1983]. From the point of view of the experimental results, however, we note that $\varrho_i$, $K_{s_i}$, $K'_{s_i}$ and $\Delta e_i^{\beta-\alpha}$ trade-off in such a way that a model consisting of a lower $\varrho_i$ (3900 kg/m$^3$), $K_{s_i}$ (180 GPa), and $K'_{s_i}$ (3.0), a higher $\Delta e_i^{\beta-c}$ (2.4 MJ/kg) and lower $\Delta e_i^{\beta-g}$ (2.05 MJ/kg), would also be consistent. This model also has a slightly steeper slope than that above, mainly because of the lower $\varrho_i$-$K_{s_i}$-$K'_{s_i}$ combination.

If we assume that the experimentally-constrained Di glass and crystal high pressure states represent equilibrium thermodynamic states of the same HPP, then the relation $\Delta e_i^{\beta-c} = \Delta e_i^{g-c} + \Delta e_i^{\beta-g}$ and the estimate $\Delta e_i^{g-c} \approx 0.36$ MJ/kg (i.e., the enthalpy of fusion of Di crystal at standard pressure: [*Robie et al.*, 1978]) would imply that $\Delta e_i^{\beta-c} - \Delta e_i^{\beta-g} \approx 0.36$ MJ/kg. This possibility is clearly contained within the range of values of $\Delta e_i^{\beta-c}$ and $\Delta e_i^{\beta-g}$ constrained by the $\varrho_i = 4100$ kg/m$^3$ model, although not represented by the "best-fit" values $\Delta e_i^{\beta-c} = \Delta e_i^{\beta-g} = 2.2$ MJ/kg. Perhaps the simplest explanation of this apparent discrepancy would be that the crystal Hugoniot states are not as completely transformed as the Di glass states. Note that the $\varrho_i = 3900$ kg/m$^3$ model just mentioned does however imply $\Delta e_i^{\beta-c} - \Delta e_i^{\beta-g} \approx 0.36$ MJ/kg.

Comparing the calculations displayed in each of these figures, we see that $T_{Hc}$ is most sensitive to $\varrho_i$, followed by $\Delta e_i^{\beta-c}$, and then $K_{s_i}$, and $T_{Hg}$ appears to be slightly more sensitive to $\Delta e_i^{\beta-g}$ than $\varrho_i$, over the range of parameter values shown. The magnitude of plausible $\Delta e_i^{\beta-\alpha}$ (1.7-2.7 MJ/kg, Figure 4*c*) values for both Di glass and crystal is of the same order as those estimated for other silicate and oxide dynamic phase transformations involving both solid-solid and solid-liquid transitions (e.g., 0.82 MJ/kg, $\alpha$-$SiO_2$ to stishovite, 1.6 MJ/kg, stishovite to liquid, [*Lyzenga et al.*, 1983]). Values of $\Delta e_i^{\beta-\alpha} \gtrsim 1$ MJ/kg for silicates and oxides are usually thought to imply partial or complete melting [e.g., *Lyzenga et al.*, 1983; *Boslough et al.*, 1986]. These considerations, plus the magnitude of the experimentally-constrained $\Delta e_i^{\beta-c}$ and $\Delta e_i^{\beta-g}$ values, would suggest that both Di glass and crystal experience solid-solid and solid-liquid transitions along their respective Hugoniots below 95 and 144 GPa, respectively. The solid-solid transition is likely to represent one from Di crystal or glass to a solid HP assemblage of oxides and/or perovskites. We could slightly favor a perovskite assemblage or single component on the basis of low-pressure static studies of Di [e.g., *Liu*, 1979*b*, 1987], which imply that Di may either disproportion into $CaSiO_3$ and $MgSiO_3$ perovskite phases, or possibly transform into a single cubic perovskite phase [*Liu*, 1987], above approximately 20 GPa and 730 K.

## DISCUSSION

In Table 4, we list the greybody fit and uncertainties, along with the calculated shock wave velocities, shock transit times, pressure and temperature, for each experiment. The values of $\hat{\epsilon}_S$ and $T_S$ in Table 4 for shots 140, 141, 169, and 170 are those for the GS fit with variable $\hat{\epsilon}_S$ and $T_S$; we choose this fit as representative of the other estimates, within experimental uncertainty. As discussed above, $\hat{\epsilon}_S$ for

TABLE 4. Experimental Results and Model Estimates.

| | Experimental Results | | | | | Model Estimates | | | | | |
|---|---|---|---|---|---|---|---|---|---|---|---|
| Shot | $\varrho_{i\alpha}$ kg/m$^3$ | $d$ mm | $v_{im}$ m/s | $\hat{\epsilon}_S$ | $T_S$ K | $u$ m/s | $v_H$ m/s | $a_{S_{min}}$ m$^{-1}$ | $t_{st}$ ns | $P_H$ GPa | $T_H$ K |
| 140 | 3282 | 1.868 | 5983 | 0.57 | 4215 | 10920 | 4460 | 880 | 170 | 160 | 4230 |
| | (6) | (0.010) | (60) | (0.23) | (364) | | | | | | |
| 141 | 3283 | 1.566 | 6143 | 0.09 | 4782 | 11060 | 4570 | 1060 | 140 | 167 | 4520 |
| | (6) | (0.010) | (50) | (0.20) | (356) | | | | | | |
| 169 | 3290 | 2.424 | 6048 | 0.97 | 4555 | 11000 | 4500 | 680 | 220 | 163 | 4340 |
| | (5) | (0.010) | (50) | (0.24) | (268) | | | | | | |
| 170 | 3289 | 1.970 | 5593 | 0.85 | 3508 | 10550 | 4170 | 820 | 185 | 144 | 3600 |
| | (7) | (0.010) | (50) | (0.14) | (141) | | | | | | |
| 196 | 2829 | 4.008 | 4673 | 1.00 | 3711 | 9185 | 3675 | 415 | 435 | 96 | 3760 |
| | (1) | (0.004) | (30) | (0.44) | (231) | | | | | | |
| 197 | 2827 | 3.966 | 4729 | 1.00 | 3866 | 9245 | 3715 | 420 | 430 | 98 | 3865 |
| | (1) | (0.001) | (30) | (0.39) | (208) | | | | | | |

Measurement uncertainty is indicated by values in parentheses. Variable definitions are as follows: $\varrho_{i\alpha}$, STP bulk density; $d$, sample thickness; $v_{im}$, impact velocity; $\hat{\epsilon}_S$, experimentally constrained greybody effective emissivity; $T_S$, experimentally constrained greybody absolute temperature; $u$ shock wave velocity through sample; $v_H$, shocked sample material ("particle") velocity; $a_{S_{min}}$, lower bound to greybody effective absorption coefficient; $t_{st}$, transit time of shock wave through sample; $P_H$, Hugoniot pressure; $T_H$, Hugoniot temperature.

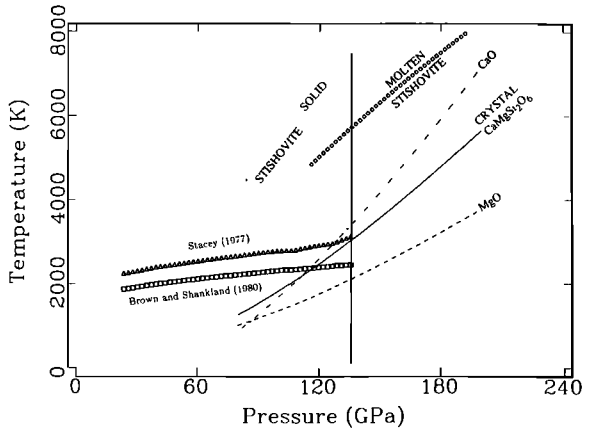


Fig. 5. Experimental and model pressure-temperature shock-compression results for HPP Di, along with experimentally constrained model results for B2-CaO [*Boslough et al.*, 1984], MgO [*Svendsen and Ahrens*, 1987], and $SiO_2$ stishovite and liquid [*Lyzenga et al.*, 1983]. Also shown are the mantle temperature profiles of *Stacey* [1977] and *Brown and Shankland* [1980]. The vertical line marks the pressure of the core-mantle boundary (136 GPa).

shots 196 and 197 are significantly greater than unity, and so we list the GS fit with $\hat{\epsilon}_S$ set to 1 as the "experimental results" for each of these shots in Table 4.

We display the TP Hugoniot for Di crystal that trisects the ranges of $\varrho_i$, $\Delta e_i^{\beta-c}$, and $K_s$, shown in Figures 4*a*-4*c* in Figure 5 (continuous curve) along with other experimental results inferred from radiation data for $SiO_2$ [*Lyzenga et al.*, 1983], CaO [*Boslough et al.*, 1986], and MgO [*Svendsen and Ahrens*, 1987]. The HPP Di results fall between the CaO and MgO results, and well below those for stishovite and liquid $SiO_2$. To first order, this is apparently due to the differences in the STP densities and compressibilities between these materials. MgO, which apparently does not experience any phase transitions below 200 GPa [*Vassiliou and Ahrens*, 1981; *Svendsen and Ahrens*, 1987] has an STP density of 3583 kg/m$^3$, B2-CaO has an STP density of about 3800-4000 kg/m$^3$ [*Jeanloz and Ahrens*, 1980*a*; *Boslough et al.*, 1984], solid HPP Di is likely to have a slightly larger $\varrho_i$ ($\approx$4100 kg/m$^3$, as discussed above) than B2-CaO, and stishovite has an STP density of $\approx$4300 kg/m$^3$. This is also true because the likely values of $\Delta e_i^{\beta-\alpha}$ for each material are approximately the same. Since B2-CaO and HPP Di apparently have very similar $\varrho_i$ values, other factors, such as compressibility, become more important. For example, B2-CaO apparently has a lower bulk modulus than solid HPP Di [*Jeanloz and Ahrens*, 1980*a*; *Boslough et al.*, 1984; *Svendsen and Ahrens*, 1983]. From (22), we see that the shock-induced temperature B2-CaO should then rise more quickly than that of HPP Di because it is more compressible; this is what we observe in Figure 5.

Also shown in Figure 5 are the (isentropic) mantle temperature profiles of *Brown and Shankland* [1980], and *Stacey* [1977]. These two models represent the range of models currently considered plausible. Note that, in placing the mantle TP curves on the same figure with the TP Hugoniots, we do not assume that these are related. Rather, the purpose here is to compare plausible mantle TP regimes with the experimentally constrained TP Hugoniot and the inferred distribution of thermodynamic phases along it. On this basis, we note that both the CaO and Di crystal Hugoniots cross the range of the model mantle geotherms in the lowermost mantle. This is the region of $D''$, which has long been known to possess distinct properties from the mantle above and core below. The possibility that $D''$ contains significant amounts of more refractory oxides and silicates (CaO, $Al_2O_3$, $CaSiO_3$, etc.) is supported by various compositional models of $D''$ constructed to be consistent with the seismic view of this region. For example, the "refractory" model of *Ruff and Anderson* [1980] contains 33 wt % CaO. From a different point of view, the work of *Svendsen and Ahrens* [1983] suggests that the $P$-$\varrho$ Hugoniot of $CaMg_{0.8}Fe_{0.2}Si_2O_6$ essentially overlaps the lower mantle Preliminary Reference Earth Model $P$-$\varrho$ profile. Both of these viewpoints suggest that the $D''$ region could contain a significantly larger amount of Ca than that ($\approx$3 wt %) expected from a chondritic viewpoint. If so, our interpretation of the Di crystal experimental results is consistent with the idea that the $CaMgSi_2O_6$ component of such a lower mantle assemblage (i.e., a mixed-oxide and/or perovskite assemblage, or possibly a single Ca,Mg-perovskite) is at least partly molten over the pressure range of the lowermost mantle. Since the finite S-wave velocity of the $D''$ region implies that it must be (at least at seismic frequencies) predominantly solid, our results further imply that such a $D''$ assemblage would have to be at a temperature below $\approx$3000 K.

## SUMMARY

We performed four experiments (140, 141, 169 and 170, Table 4), on $CaMgSi_2O_6$ (Di) single crystal, an end-member pyroxene relevant to investigations into the composition of Earth's mantle, and two experiments on Di glass (196 and 197, Table 4) with a density 86% that of Di crystal. The targets consisted of a Ta driver plate, Ag film layer, and sample layer. We recorded the intensity of radiation from the target as a function of time at 450-, 600-, 750-, and 900-nm wavelengths. This radiation is first observed when the shock wave compresses the Ag film at the Ag-sample interface ($t_o$, Figure 2*a* or 2*b*). In all experiments, the observed radiation intensity rises sharply to a peak value, and then, as the shock wave propagates into the sample, it decays almost as quickly to an approximately time independent value. This occurs over 100-110 ns (Figure 2*a*) to the radiation intensity from Di glass targets and over 20-30 ns (Figure 2*b*) to the radiation intensity from Di crystal targets. We conclude that the strong decay of the initial radiation intensity is controlled by $\tau_S(t)$ and reflects an increase in the optical absorption of Di upon shock compression ($a_S \geq$ 500–1000 m$^{-1}$ >> $a_{US}$).

Greybody fits to the radiation intensity of shocked Di crystal (diopside) constrain shock induced temperatures for this starting material of 3500-4800 K in the 145-170 GPa range. Similar fits to the radiation intensity of shocked Di glass imply that it achieves shock induced temperatures of 3600-3800 K in the 96-98 GPa pressure range.

Using linear $u$-$v_H$ relations for Ta, Ag, and Di crystal, we calculate Hugoniot states for Di crystal and compare them, for a range of parameter values, to the experimental results. Having no experimentally constrained $u_g$-$v_{Hg}$ relation for Di glass, we calculate one from the STP densities of Di glass and crystal, the experimentally constrained $u_c$-$v_{Hc}$ relation of Di crystal, the difference in specific internal energy between the glass and crystal states at STP, and the

STP properties of the HPP, via a relation between the glass and crystal Hugoniots at a given density, as discussed in the text. These calculations suggest that the temperature of the shock-compressed state for Di crystal is most sensitive to $\varrho_i$, followed by $\Delta e_i^{\beta-c}$, and then $K_{s_i}$. The shock-induced temperatures of Di glass appear to be more sensitive to $\Delta e_i^{\beta-g}$ than $\varrho_i$ in the respective parameter ranges of interest. Comparison of the experimentally constrained TP Di crystal Hugoniot with those of its constituent oxides ($SiO_2$, CaO and MgO) demonstrates the primary influence of the STP density and compressibility of these materials on the temperature of their shock-compressed states. The experimentally constrained HPP Di TP Hugoniot falls between those of CaO and MgO, and well below those for stishovite and liquid $SiO_2$.

Calculated shock-compressed states for these materials, when compared to the experimental results, imply that Di crystal high-pressure states in the 145-170 GPa range represent the liquid state with an STP density of 4100±100 kg/m$^3$, STP bulk modulus of 250±50 GPa and STP HPP–initial phase specific internal energy difference of 2.2±0.5 MJ/kg. These results are consistent with the density of $CaO$-$MgO$-$SiO_2$ oxide, $CaSiO_3$-$MgSiO_3$ perovskite assemblages, or possibly $CaMgSi_2O_6$ perovskite [*Liu*, 1987]. Di glass Hugoniot states in the range 96-98 GPa are consistent with the same "best-fit" HPP STP properties, implying that it as well is at least partially, if not completely, melted at these pressures along its Hugoniot.

The Di crystal Hugoniot constrained by the experimental results lies in the range 2500-3000 K between 110 and 135 GPa, within the plausible range of lowermost mantle temperature profiles. The possibility of a significant Ca oxide or silicate component in the lower mantle, combined with our interpretation of the Di crystal experimental results, implies that such a $D''$ region would have to be at a temperature below ≈3000 K.

## APPENDIX

In this appendix, we establish (21), the relation between the crystal and porous/glass Hugoniots, and then detail the calculations for $a_{ig}$ and $b_{ig}$ developed via (20) written for Di glass and crystal, and (21). Relation (21) is actually a special case of a more general relation which is valid for any two distinct initial ($P = P_i$) forms, or states, of the same material shock-compressed into the same high-pressure phase ($\beta$). Let $T_{i1}$, $s_{i1}$, and $\varrho_{i1}$ be the temperature, specific entropy, and mass density, respectively, of the first initial state, and $T_{i2}$, $s_{i2}$, and $\varrho_{i2}$ the analogous quantities for the second initial state. These two states may be, for example, different phases at the same pressure (e.g., solid and liquid), or a porous material and its crystal counterpart at the same pressure. We assume that each initial state shock compresses adiabatically to a high-pressure state in thermodynamic equilibrium. Further, we assume that both the initial and shocked states are ideal fluids. Under these assumptions, the change in specific internal energy, $e(s, \varrho)$, of either initial state upon shock compression is given by the Rankine-Hugoniot relation [e.g., *Rice et al.*, 1958]:

$$e(s_{H\alpha}, \varrho_{H\alpha}) - e(s_{i\alpha}, \varrho_{i\alpha}) = \frac{1}{2\varrho_{i\alpha}}\eta_\alpha[P_{H\alpha} + P_i] \qquad \text{(A1)}$$

with $\alpha = 1, 2$, and $\eta_\alpha = 1 - \varrho_{i\alpha}/\varrho_{H\alpha}$, as used in the text. Assuming that shock compression separates states in thermodynamic equilibrium, we may follow *McQueen et al.* [1967], and *Ahrens et al.* [1969], in constructing an equivalent thermodynamic path to (A1) for either initial state:

$$e(s_{H\alpha}, \varrho_{H\alpha}) - e(s_{i\alpha}, \varrho_{i\alpha}) = \Delta e_i^{\beta-\alpha} + \Delta e_{s_i} + \Delta e_{\varrho_{H\alpha}} \qquad \text{(A2)}$$

with $\Delta e_{\varrho_{H\alpha}} = e(s_{H\alpha}, \varrho_{H\alpha}) - e(s_i, \varrho_{H\alpha})$. Combining (A1) and (A2), we obtain

$$\frac{1}{2\varrho_{i\alpha}}\eta_\alpha[P_{H\alpha} + P_i] = \Delta e_i^{\beta-\alpha} + \Delta e_{s_i} + \Delta e_{\varrho_{H\alpha}} \qquad \text{(A3)}$$

for $\alpha = 1, 2$. Now, if we shock both initial states into the same high-pressure phase ($\beta$) at the same density $\varrho_H = \varrho_{H1} = \varrho_{H2}$, we may combine (A3) written for initial state 1 with (A3) written for initial state 2 by eliminating $\Delta e_{s_i}$ between $\Delta e_{i1}$ and $\Delta e_{i2}$. Doing this, we obtain

$$\eta_2 P_{H2} = (1 - \phi)\eta_1 P_{H1} - \phi P_i + 2\varrho_{i2}(\Delta e_H^{2-1} - \Delta e_i^{2-1}) \qquad \text{(A4)}$$

with $\phi = 1 - \varrho_{i2}/\varrho_{i1}$, $\Delta e_i^{2-1} = e(s_{i2}, \varrho_{i2}) - e(s_{i1}, \varrho_{i1})$, and

$$\Delta e_H^{2-1} = e(s_{H2}, \varrho_H) - e(s_{H1}, \varrho_H)$$

Assuming that $\gamma$, the equilibrium thermodynamic Grüneisen's parameter of $\beta$, is a function of density alone, the relation

$$\rho\gamma\left(\frac{\partial e}{\partial P}\right)_\rho = 1 \qquad \text{(A5)}$$

gives us

$$\Delta e_{\varrho_{H\alpha}}^{2-1} = \frac{1}{\varrho_H \gamma_H}[P_{H2} - P_{H1}] \qquad \text{(A6)}$$

with $\gamma_H = \gamma(\varrho_H)$. Substituting this into (A5) and rearranging, we obtain

$$P_{H2} = \frac{(1 - \phi)}{\mathcal{D}_2}[\mathcal{D}_1 P_{H1} + \gamma_H k] \qquad \text{(A7)}$$

with $\mathcal{D}_\alpha = 1 - (1 + \frac{1}{2}\gamma_H)\eta_\alpha$ ($\alpha = 1, 2$), and

$$k = \varrho_{i2}\Delta e_i^{2-1} + \frac{1}{2}\phi P_i$$

With initial state 1 as Di crystal, and initial state 2 as Di glass, (A7) corresponds to (21) in the text. To our knowledge, the particular use to which we put (A7) in the text is novel; perhaps the most common use of (A7), or relations like it, is to estimate $\gamma_H$ from porous and crystal shock compression data:

$$\gamma_H = \frac{2(1 - \eta_2)[P_{H2} - P_{H1}]}{2\varrho_{i2}\Delta e_i^{2-1} + \phi[P_{H1} + P_i] + \eta_2[P_{H2} - P_{H1}]} \qquad \text{(A8)}$$

when $P_{H2}(\varrho_H)$ and $P_{H1}(\varrho_H)$ are independently constrained; usually, the approximation $\Delta e_i^{2-1} = 0$ is used [e.g., *Jeanloz*, 1979].

Having established (20), we are now in a position to calculate $a_{ig}$ and $b_{ig}$. The basic idea here is that we require (21), and (20) written for Di glass, to be consistent descriptions of Di glass $P_{Hg}$-$\varrho_{Hg}$ relations. We do this numerically by generating a Di glass Hugoniot using (21) and then fitting (20) written for Di glass to this calculated Hugoniot via the LM method discussed in the text to find the minimum of the $\chi^2$ statistic

$$\chi^2(a_{ig}, b_{ig}) = \sum\nolimits_n [P_{sdat}(\varrho_H^{(n)}) - P_{mod}(\varrho_H^{(n)}; a_{ig}, b_{ig})]^2 \qquad \text{(A9)}$$

As just explained, $P_{mod}(\varrho_H^{(n)}; a_{ig}, b_{ig})$ is given by (20) written for Di glass, while $P_{sdat}(\varrho_H^{(n)})$ is given by (21). Via this latter dependence, the calculated Di glass Hugoniot, and so the fit, then depends on the set

$$\{P_i, \Delta e_i^{g-c}, \varrho_{ig}, \varrho_{ic}, a_{ic}, b_{ic}, \varrho_i, \gamma_i\} \qquad \text{(A10)}$$

of parameters which remain fixed during the fit. All of these except $P_t = 0.1$ MPa and $\Delta e_i^{g-c} = 0.36$ MJ/kg (i.e., the enthalpy of fusion of Di crystal at standard pressure: [*Robie et al.*, 1978]) appear in Table 3, all except $\varrho_i$ and $\gamma_i$ are well-constrained, and the dependence of the fit on these last two over the ranges of interest was negligible. We carried out the fit for densities between $\varrho_t$ (≈45 GPa) and 5500 kg/m$^3$ (≈200 GPa). The fit was basically insensitive to the number of calculated Di glass Hugoniot points used, and the largest single value of $P_{sdat}(\varrho_H^{(n)}) - P_{mod}(\varrho_H^{(n)}; a_{ig}, b_{ig})$ in the range 45-200 GPa was 3 GPa, which occured at 200 GPa, and which we used as an uncertainty when plotting the data in Figures 4*a*-4*c*. The growth of the deviation between the calculated Di glass Hugoniot and model with increasing density reflects both a worsening of the fit and the linear shock velocity-material velocity approximation (19) for Di glass ($b_{ig}\eta_g = 0.67$ at 200 GPa).

*Acknowledgements.* We thank Papo Gelle, Mike Long, Chuck Manning and Leon Young for experimental asssistance, and Jay D. Bass, Gregory Miller, Douglas R. Schmitt, and James A. Tyburczy for enlightening discussions. We also thank James A. Tyburczy and two anonymous individuals for reviewing and improving the first version of this paper. Support under NASA and NSF grants NGL-05-001-205 and EAR-86-08249, respectively, is gratefully acknowledged. Contribution 4480, Division of Geological and Planetary Sciences, California Institute of Technology, Pasadena, California.

## REFERENCES

Ahrens, T. J., J. T. Rosenberg, and M. H. Ruderman, Dynamic properties of rocks, *Final Rep. DA-45-146-XZ-277*, SRI project FGU-4816, Standford Res. Inst., Standford, Calif., September, 1966.

Ahrens, T. J., D. L. Anderson, and A. E. Ringwood, Equations of state and crystal structures of high-pressure phases of shocked silicates and oxides, *Rev. Geophys., 7*, 667-707, 1969.

Bass, J. D., B. Svendsen, and T. J. Ahrens, The temperatures of shock compressed iron, in *Mineral Physics*, edited by M. H. Manghnani and Y. Syono, pp. 393-402, Scientific, Tokyo, 1987.

Binsted, N., G. N. Greaves, and C. M. B. Henderson, An EXAFTS study of glassy and crystalline phases of compositions $CaAl_2Si_2O_8$ and $CaMgSi_2O_6$, *Contrib. Mineral. Petrol., 89*, 103-109, 1985.

Boslough, M. B., Shock wave properties and high pressure equations of state of geophysically important materials, Ph.D. dissertation, 171 pp., Calif. Inst. Technol., Pasadena, 1984.

Boslough, M. B., A model for time dependence of shock induced thermal radiation of light, *J. Appl. Phys., 56*, 3394-3399, 1985.

Boslough, M. B., T. J. Ahrens, and A. C. Mitchell, Shock temperatures in CaO, *J. Geophys. Res., 89*, 7845-7851, 1984.

Boslough, M. B., T. J. Ahrens, and A. C. Mitchell, Shock temperatures in anorthite glass, *Geophys. J. R. Astron. Soc., 84*, 475-489, 1986.

Brown, J. M., and T. Shankland, Thermodynamic parameters of the Earth as determined from seismic profiles, *Geophys. J. R. Astron. Soc., 66*, 579-596, 1980.

Grossman, L., and J. W. Larimer, Early chemical history of the solar system, *Rev. Geophys., 12*, 71-101, 1974.

Grover, R., and P. A. Urtiew, Thermal relaxation at interfaces following shock compression, *J. Appl. Phys., 45*, 146-152, 1974.

Jeanloz, R., Properties of iron at high pressure and the state of the core, *J. Geophys. Res., 84*, 6059-6069, 1979.

Jeanloz, R., and T. J. Ahrens, Equations of state of FeO and CaO, *Geophys. J. R. Astron. Soc., 62*, 505-528, 1980*a*.

Jeanloz, R., and T. J. Ahrens, Anorthite: thermal equation of state to high pressures, *Geophys. J. R. astr. Soc., 62*, 529-549, 1980*b*.

Kondo, K. E., and T. J. Ahrens, Heterogeneous shock induced thermal radiation in minerals, *Phys. Chem. Miner., 9*, 173-181, 1983.

Kormer, S. B., Optical study of the characteristics of shock compressed condensed dielectrics, *Sov. Phys. Usp.*, Engl. Trans., *11*, 229-254, 1968.

Liu, L. G., A new high pressure phase of $CaAl_2Si_2O_8$ and implications for Earth's interior, *Earth Planet. Sci. Lett., 40*, 401-406, 1978.

Liu, L. G., High pressure phase transformations in the system $CaSiO_3$-$Al_2O_3$, *Earth Planet. Sci. Lett., 43*, 331-335, 1979*a*.

Liu, L. G., The system enstatite-wollastonite at high pressures and temperatures, with emphasis on diopside, *Phys. Earth Planet. Inter., 19*, P15-P18, 1979*b*.

Liu, L. G., New silicate perovskites, *Geophys. Res. Lett., 14*, 1079-1082, 1987.

Lyzenga, G. A., Shock temperatures of materials: experiments and applications to the high pressure equation of state, Ph.D. dissertation, 201 pp., Calif. Inst. Technol., Pasadena, 1980.

Lyzenga, G. A., T. J. Ahrens, and A. C. Mitchell, Shock temperatures of $SiO_2$ and their geophysical implications, *J. Geophys. Res., 88*, 2431-2444, 1983.

Marsh, S. P., *LASL Shock Hugoniot Data*, 658 pp., University of California Press, Berkeley, 1980.

McQueen, R. G., S. P. Marsh, and J. N. Fritz, Hugoniot equation of state of twelve rocks, *J. Geophys. Res., 72*, 4999-5036, 1967.

Mitchell, A. C., and W. J. Nellis, Shock compression of aluminum, copper, and tantalum, *J. Appl. Phys., 52*, 3363-3374, 1984.

Pastine, D. J., D. Piacesi, The existence and implications of curvature in the relation between shock and particle velocities for metals, *J. Chem. Phys. Solids*, 1783-1792, 1966.

Press, W. H., B. P. Flannery, S. A. Teukolsky, and W. T. Vetterling, *Numerical Recipies: The Art of Scientific Computing*, 818 pp., Cambridge University Press, New York, 1986.

Rice, W. H., R. G. McQueen, and J. M. Walsh, Compressibility of solids by strong shock waves, *Solid State Phys., 6*, 1-63, 1958.

Robie, R. A., B. S. Hemingway, and R. J. Fisher, Thermodynamic properties of minerals and related substances at 298.15 K and 1 bar ($10^5$ Pascals) pressure and at higher temperatures, U.S. Geol. Surv. Bull., 1452, 456 pp., 1978.

Ruff, L. J., and D. L. Anderson, Core formation, evolution and convection: a geophysical model, *Phys. Earth Planet. Inter., 21*, 181-201, 1980.

Schmitt, D. R., and T. J. Ahrens, Temperatures of shock-induced shear instabilities and their relationship to fusion curves, *Geophys. Res. Lett., 10*, 1077-1080, 1983.

Schmitt, D. R., B. Svendsen, and T. J. Ahrens, Shock induced radiation from minerals, in *Shock Waves in Condensed Matter-1985*, edited by Y. M. Gupta, pp. 261-266, Plenum, New York, 1986.

Stacey, F., A thermal model of the earth, *Phys. Earth. Planet. Inter., 15*, 341-348, 1977.

Stevenson, D. J., Models of the earth's core, *Science, 214*, 611-618, 1981.

Svendsen, B., and T. J. Ahrens, Dynamic compression of diopside and salite to 200 GPa, *Geophys. Res. Lett., 10*, 501-504, 1983.

Svendsen, B., and T. J. Ahrens, Shock induced temperatures of MgO, *Geophys. J. R. Astron. Soc., 91*, 667-691, 1987.

Svendsen, B., J. D. Bass, and T. J. Ahrens, Optical radiation from shock compressed materials and interfaces, *Phys. Rep., 180*, 333-423, 1989.

Turekian, K. K., and S. P. Clark, Jr., Inhomogeneous accretion model of the Earth from the primitive solar nebula, *Earth Planet. Sci. Lett., 6*, 346-348, 1969.

Urtiew, P. A., and R. Grover, Temperature deposition caused by shock interactions with material interfaces, *J. Appl. Phys., 45*, 140-145, 1974.

Vassiliou, M. S., and Ahrens, T. J., Hugoniot equation of state of periclase to 200 GPa, *Geophys. Res. Lett. 8*, 729-732, 1981.

B. Svendsen, Fachbereich 6, Mechanik, Technische Hochschule Darmstadt, D-6100 Darmstadt, West Germany.

T. J. Ahrens, Seismological Laboratory, California Institute of Technology, Pasadena, CA 91125.

(Received June 19, 1987;
revised July 19, 1988;
accepted October 27, 1988.)